



# Superoleophobic surface modification for robust membrane distillation performance



Nick Guan Pin Chew<sup>a,b,1</sup>, Shanshan Zhao<sup>b,1</sup>, Chandresh Malde<sup>c</sup>, Rong Wang<sup>b,d,\*</sup>

<sup>a</sup> Interdisciplinary Graduate School, Nanyang Technological University, Singapore 639798, Singapore

<sup>b</sup> Singapore Membrane Technology Centre, Nanyang Environment and Water Research Institute, Nanyang Technological University, Singapore 637141, Singapore

<sup>c</sup> Johnson Matthey Technology Centre, Reading RG4 9NH, United Kingdom

<sup>d</sup> School of Civil and Environmental Engineering, Nanyang Technological University, Singapore 639798, Singapore

## ARTICLE INFO

### Keywords:

Polydopamine  
Polyethylenimine  
Membrane distillation  
Surface modification  
Produced water

## ABSTRACT

Inspired by mussels' byssus with remarkable adhesive power that is neither degraded nor deformed in the marine environment, dopamine coating has emerged as an option for membrane surface modification. With its many advantages, direct-contact membrane distillation (DCMD) appears to hold potential for the recovery of high quality water from produced water. However, membrane fouling and pore wetting are challenging issues of long-term DCMD operations due to the presence of oils and surfactants in these waters. Hence, it is paramount to develop robust membranes with anti-fouling and anti-wetting properties for effective produced water treatment. In this study, we fabricated a composite hollow fiber membrane by single-step co-deposition of polydopamine (PDA)/polyethylenimine (PEI) onto the outer surface of a commercial hydrophobic polyvinylidene fluoride (PVDF) substrate. The successful co-deposition was verified using different characterization techniques. The composite membrane exhibited Janus wettability (Janus membranes have opposing properties at an interface) with its modified outer surface being in-air hydrophilic/underwater superoleophobic for preventing organics adhesion while insuring that unmodified pores beneath the surface remained hydrophobic for vapor transport. The anti-fouling and anti-wetting properties of the modified membrane were investigated via DCMD experiments by feeding a series of low surface tension solutions. In comparison to the pristine PVDF membrane, the modified membrane exhibited promising wetting resistant property against different surfactant types and excellent fouling resistant property against nonionic and cationic surfactants. Moreover, the modified membrane presented a promising long-term performance when feeding a cationic surfactant-stabilized petroleum-in-water emulsion mimicking produced water, during which a stable flux and excellent permeate quality were maintained throughout 7 days of operation. The efficacious combined effects of a hydration layer and protonated amine-functional groups on the PDA/PEI grafted layer could prevent membrane fouling and pore wetting. The results suggest that the mussel-inspired composite PVDF membrane could potentially be used for long-term water recovery from produced water via DCMD.

## 1. Introduction

The importance of oil and gas in today's context cannot be overstated as they continue to account for nearly 78% of the world's total energy consumption [1]. With many production activities, a substantial volume of produced water is generated annually within the oil and gas industry, making it one of the most water-intensive industries. Managing produced water has become a consequential part of the sustainable development of the oil and gas industry due to stringent environmental legislations, severe strain on water resources, and escalating costs of

wastewater disposal [2]. Amongst numerous management methods, the reuse of produced water is a growing trend as it provides a potential profit stream [3]. To tap on this potential, produced water has to be first treated to remove main constituents such as oils and greases, production chemicals (surfactants), and production solids (salts).

Membrane distillation (MD) is an emerging thermally driven separation process using a hydrophobic porous membrane as a selective barrier against liquid transport. In the MD process, the transport of water vapor molecules through the membrane pores is driven by the partial vapor pressure difference resulting from the temperature

\* Corresponding author at: Singapore Membrane Technology Centre, Nanyang Environment and Water Research Institute, Nanyang Technological University, Singapore 637141, Singapore.

E-mail address: [rwang@ntu.edu.sg](mailto:rwang@ntu.edu.sg) (R. Wang).

<sup>1</sup> These authors contributed equally to this work.

difference between the hot feed and the cold permeate [4–6]. Highly purified distillate is produced when the vapor molecules condense on the cold permeate side, while most of the nonvolatile species are rejected. MD has a couple of distinct advantages over other pressure-driven membrane processes that include its ability to treat wastewater with high salinity and utilize low-grade thermal energy, which is an abundant available source of emission-free power in the oil and gas industry [7–14]. From the economic perspective, MD's small footprint and low operating cost render it a leading candidate for small-scale and off-grid applications for water recovery from produced water [15].

Polyvinylidene fluoride (PVDF) is one of the most extensively used polymeric materials for MD operations ascribing to its excellent thermal stability, chemical stability, and mechanical strength. However, hydrophobic PVDF membranes are especially vulnerable to fouling caused by the adsorption of hydrophobic species (e.g. oil) and/or amphiphiles (e.g. surfactants). Adsorption can be through either hydrophobic interactions or electrostatic interactions between the foulants and membrane surface. Besides membrane fouling, pore wetting also remains a huge challenge faced in long-term MD operations for produced water treatment due to the presence of low surface tension substances (e.g. natural or add surfactants). These substances can significantly reduce the liquid entry pressure (LEP) of the membrane pores, compromising on the permeate flux and salt selectivity of the membrane. Moreover, it has been proven that membrane fouling is the main contributor to pore wetting [16]. Therefore, it is paramount to develop robust MD membrane with both anti-fouling and anti-wetting properties in long-term operations for water recovery from produced water.

Minimizing pore wetting and fouling of PVDF membranes concurrently have proven to be challenging. A wide range of surface modification methods has been adopted to achieve this goal. For example, Yuan et al. fabricated PVDF membranes with superhydrophobic surfaces that exhibited minimal pore wetting [17–19]. However, these superhydrophobic surfaces might remain susceptible to fouling and sensitive towards low surface tension feeds [20–22]. As a result, these membranes might not be suitable for long-term MD operations for produced water treatment. Inspired from biological surfaces such as fish scales, clamshell, and sharkskin in the natural world, materials scientists have found that their underwater superoleophobic surfaces could be the key to resisting organic fouling and microorganism adhesion in the marine environment [23–26]. Therefore, engineering membrane surfaces with underwater superoleophobicity property has emerged as an effective strategy to prevent oil fouling in MD applications such as produced water treatment [27–29]. Generally, two aspects that include the hierarchical surface structure and hydrophilic surface chemistry are key requirements for fabricating such surfaces [30–37]. By following this principle, numerous composite MD membranes with asymmetric wetting properties have been developed. These membranes consist of a hydrophilic/underwater oleophobic top surface for preventing organics

adhesion and a hydrophobic substrate for vapor transport. For example, a composite PVDF membrane with a hydrophilic surface was developed by plasma-induced deposition of polyethylene glycol and  $\text{TiO}_2$  nanoparticles, exhibiting good resistance against both wetting and mineral oil fouling [38]. In recent studies, PVDF membranes with underwater superoleophobic property were prepared by spray coating of various nanocomposite layers with sophisticated micro/nano-hierarchical structures to repel the adsorption of physically emulsified crude oil [27,29]. Even though significant progress has been made to develop these composite membranes to minimize oil adhesion and pore wetting, they have not realized the full potential of long-term MD operations with low surface tension feeds from industries. Moreover, previous membrane surface modification methods often involve several steps to create a hydrophilic layer with hierarchical structures, which may be too complex for real applications. Therefore, there is an urgent need to develop a facile method to engineer membrane surfaces that can achieve robust long-term MD performance when handling low surface tension wastewaters.

Over the last decade, the mussel-inspired chemistry of dopamine has been widely used for a variety of surface modifications due to its unique advantages of material-independent attachment and surface post-functionalization [39]. Compared with physical coating, the resulting polydopamine (PDA) coating has stronger binding affinity to the membrane surface [40]. Moreover, co-deposition of dopamine with other molecules such as polyethylenimine (PEI) can greatly increase the stability of the grafted layer under harsh conditions [41]. As a result, this versatile and robust technique has been adopted in a broad range of membrane processes such as microfiltration [42–45], ultrafiltration [46,47], nanofiltration [48], and forward osmosis [49,50] for various purposes such as improving anti-fouling performance and enhancing structural stability.

This study aims at developing robust membrane surfaces with anti-fouling and anti-wetting properties to be used in direct-contact membrane distillation (DCMD) operations for water recovery from produced water. Specifically, a composite membrane with Janus wetting properties was fabricated by single-step co-deposition of the hydrophilic PDA/PEI layer on the outer surface of a hydrophobic PVDF hollow fiber substrate. Janus membranes have asymmetric properties on either side of the membrane [51]. The surface chemistry, wetting properties, and structure of the modified PVDF membrane were studied comprehensively. Subsequently, bench-scale DCMD experiments were carried out using a series of low surface tension feeds including various types of surfactant solutions and surfactant-stabilized oil-in-water (O/W) emulsions. The performances of the modified PVDF membrane were analyzed and compared against those of the pristine PVDF membrane to ascertain its suitability and robustness for long-term produced water treatment. To the best of our knowledge, this is the first report about the co-deposition of PDA/PEI on a hydrophobic PVDF hollow fiber

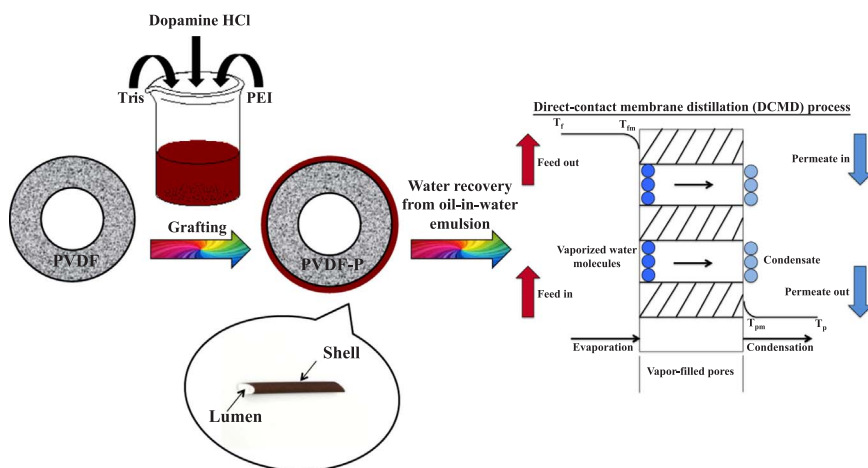


Fig. 1. Schematic of co-deposition of PDA/PEI on the outer surface of a PVDF membrane and its application in water recovery from oil-in-water emulsions via DCMD.

substrate that can be used for DCMD applications against low surface tension feeds.

## 2. Experimental

### 2.1. Materials and chemicals

Dopamine hydrochloride (DA), PEI (Mw = 800), tris(hydroxymethyl)aminomethane (Tris), sodium dodecyl sulfate (SDS), dodecyltrimethylammonium bromide (DTAB), and petroleum (~ 18% aromatics) were purchased from Sigma-Aldrich (Singapore). Sodium chloride (NaCl, 99.5%), sorbitan monolaurate (Span® 20), and polyoxyethylenesorbitan monolaurate (Tween® 20) were purchased from Merck Millipore (Singapore). Hydrophobic PVDF hollow fiber membranes with a nominal pore size of 0.027 μm were obtained from a commercial supplier. These membranes were used as substrates for surface modification and as references for the fouling and wetting experiments. Milli-Q® water with a resistivity value of 18.2 MΩ cm was used in all experiments (produced by the Milli-Q® integral water purification system, Merck Millipore).

### 2.2. Fabrication of composite PVDF hollow fiber membrane

The in-air hydrophilic/underwater superoleophobic composite membrane was fabricated by co-deposition of PDA/PEI on a hydrophobic PVDF substrate, which is illustrated in Fig. 1. Firstly, 2 g L<sup>-1</sup> of DA and 50 mM of Tris were weighed and dissolved into 2 g L<sup>-1</sup> of PEI solution. Similar procedures have been reported elsewhere [42,52,53]. After that, the pristine PVDF membranes were immersed in the PDA/PEI solution with shaking at 40 rpm for a certain time (Orbital Maxi MD Humidity, OVAN, Spain). Precautions were taken to ensure that only the outer surfaces of the hydrophobic PVDF hollow fibers were modified, so that the membrane pores beneath the surface remained hydrophobic for vapor transport. Finally, the composite membranes were rinsed thoroughly with Milli-Q® water and freeze-dried overnight (Alpha 2–4, Martin Christ, Germany). Hereon, the PDA/PEI coated PVDF membrane will be referred to as PVDF-P membrane. Lab-scale modules were prepared by sealing 5 pieces of 18 cm long hollow fiber in Teflon tubing. A new membrane module was prepared for each experiment. The effective membrane area for each module was 43 cm<sup>2</sup>.

### 2.3. Membrane characterizations

The differences in the surface and cross-section morphologies of the pristine PVDF and PVDF-P membranes were observed using a field emission scanning electron microscope (FESEM) (JSM-7200F, JEOL,

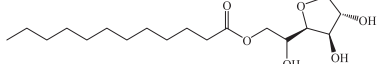
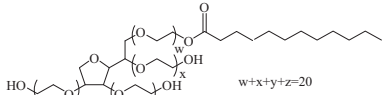
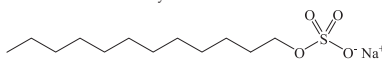
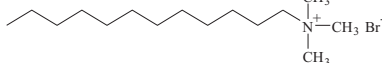
Japan). The dried hollow fibers were fractured in liquid nitrogen and then sputter-coated with a layer of platinum by a sputter coater (JEC-3000FC, JEOL, Japan) prior to the respective tests. The outer surface topographies and roughness of the pristine PVDF and PVDF-P membranes were observed through an atomic force microscope (AFM) (XE-100, Park Systems, Korea) with a scan area of 5 μm × 5 μm under the tapping mode. The pore size distributions and mean pore sizes of the pristine PVDF and PVDF-P membranes were analyzed by a capillary flow porometer (CFP-1500A, Porous Materials, Inc., USA). The hollow fiber membranes were glued to the sample holders using epoxy and wetted thoroughly by Galwick™, a low surface tension wetting fluid. The detailed underlying working principles and experimental procedures had been described in our previous research works [4,54].

The surface functional groups of the pristine PVDF and PVDF-P membranes were qualitatively analyzed by a Fourier transform infrared spectroscope via attenuated total reflectance mode (ATR-FTIR) (IR-Prestige-21, Shimadzu, Japan) over a scan range of 400–4000 cm<sup>-1</sup> with a resolution of 4 cm<sup>-1</sup>. The elemental compositions of the outer and inner surfaces of the pristine PVDF and PVDF-P membranes were measured using an X-ray photoelectron spectroscope (XPS) (AXIS Supra™, Kratos Analytical, UK) with a 500 mm Rowland circle monochromic Al Kα excitation source at 1486.7 eV. An emission current of 5 mA and operating voltage of 15 kV were employed. High-resolution spectra were collected using pass energies of 20 eV and 160 eV for narrow and broad scans, respectively. The sampling depth was approximately 10 nm with a takeoff angle of 0° with respect to the membrane surface. All binding energies for the elements of interest were corrected against an adventitious C 1s core level at 285.0 eV. All XPS peaks were fitted using the Shirley background together with the Gaussian-Lorentzian function by the CASA XPS software.

The dynamic water contact angles of the pristine PVDF and PVDF-P membranes were determined by a tensiometer (DCAT11, DataPhysics, Germany), according to the Wilhelmy method. A hollow fiber membrane taped to a sample holder was hung from the arm of an electrobalance and underwent through three cycles of immersion into Milli-Q® water at an immersion depth of 5 mm, with the surface detection threshold set at 0.5 mg. Each membrane sample was measured ten times and an average value was calculated. The underwater oleophilicity and oleophobicity of the pristine PVDF and PVDF-P membranes were evaluated using the captive bubble method via a goniometer (OCA 25, DataPhysics, Germany). In this method, a drop of petroleum was injected beneath the membrane taped onto a cell underwater. The interactions between the oil droplet and the respective membrane surfaces were observed.

The surface zeta potentials of the pristine PVDF and PVDF-P membranes were determined using an electrokinetic analyzer (SurPASS™ 3,

**Table 1**  
Properties of surfactants used in this study.

Surfactant	Molecular weight (g mol <sup>-1</sup> )	HLB <sup>a</sup>	Surface tension <sup>b</sup> (mN m <sup>-1</sup> )	Chemical structure
Span® 20	346.5	8.6 [56]	~ 25 ± 0.12	
Tween® 20	1227.5	16.7 [56]	~ 36 ± 0.25	
SDS	288.4	40.0 [57]	~ 30 ± 0.17	
DTAB	308.3	24.3 [58]	~ 40 ± 0.22	

<sup>a</sup> Hydrophilic-Lipophilic Balance.

<sup>b</sup> Surface tension was measured at 50 mg L<sup>-1</sup> in 3.5 wt% NaCl using tensiometer (DCAT11, DataPhysics, Germany).

Anton Paar, Austria) based on streaming potential measurements. 1 mM NaCl was prepared as the background electrolyte solution. 0.05 M HCl and NaOH were used for pH titration. Hollow fiber membranes were flattened and taped onto two sample holders mounted in an adjustable gap cell (20 mm × 10 mm). The gap height was adjusted to ~ 100 μm. The NaCl electrolyte solution flowed across the cell through pressurization of the liquid reservoir from 200 mbar to 600 mbar, causing electric charge separation. The resulting potential difference was detected and calculated using the Helmholtz-Smoluchowski equation [55].

To evaluate the structural stability of the grafted layer on the PVDF-P membrane, the membrane sample was ultrasonic treated for 10 min at ambient temperature in an ultrasonic bath (FB 15068, Fisher Scientific, USA) with a frequency of 37 kHz.

#### 2.4. Preparation and characterization of surfactant solutions and DTAB-stabilized petroleum-in-water emulsion

Different saline feeds with low surface tension were prepared for the DCMD experiments, including four surfactant solutions that were prepared by mixing 50 mg L<sup>-1</sup> of Span® 20, Tween® 20, SDS, and DTAB in 3.5 wt% NaCl solution, respectively. The properties of these surfactants are listed in Table 1. Separately, DTAB-stabilized petroleum-in-water

emulsion was prepared by mixing 450 mg L<sup>-1</sup> of petroleum, 50 mg L<sup>-1</sup> of DTAB, and 8 L of 3.5 wt% NaCl solution in a high speed heavy-duty blender (CB15, Waring® Commercial, USA) for at least 3 min. The composition of the emulsion was modeled as closely to real produced water samples as possible. Petroleum, DTAB, and NaCl were used to represent the oil, surfactant, and dissolved solids present in produced water, respectively. The oil droplet size distribution of the emulsion was measured by a mastersizer (Hydro2000SM, Malvern Instruments, UK) while its zeta potential was measured by a zetasizer (NanoZS, Malvern Instruments, UK). Fresh emulsions were prepared after every 24 h of operation to ensure that the feed remained kinetically stable because unstable emulsions might not accurately demonstrate the fouling and wetting behaviors of both the pristine PVDF and PVDF-P membranes.

#### 2.5. DCMD performance tests

The fouling and wetting behaviors of the pristine PVDF and PVDF-P membranes were systematically studied via a DCMD experimental rig as illustrated in our previous work [4]. The feed and permeate solutions were maintained at 333 K and 293 K, respectively, and circulated in a countercurrent flow configuration at 0.7 L min<sup>-1</sup> and 0.25 L min<sup>-1</sup>, respectively. For both sets of membranes, the feed was flowed on the shell of the hollow fibers while the permeate was flowed in the lumen.

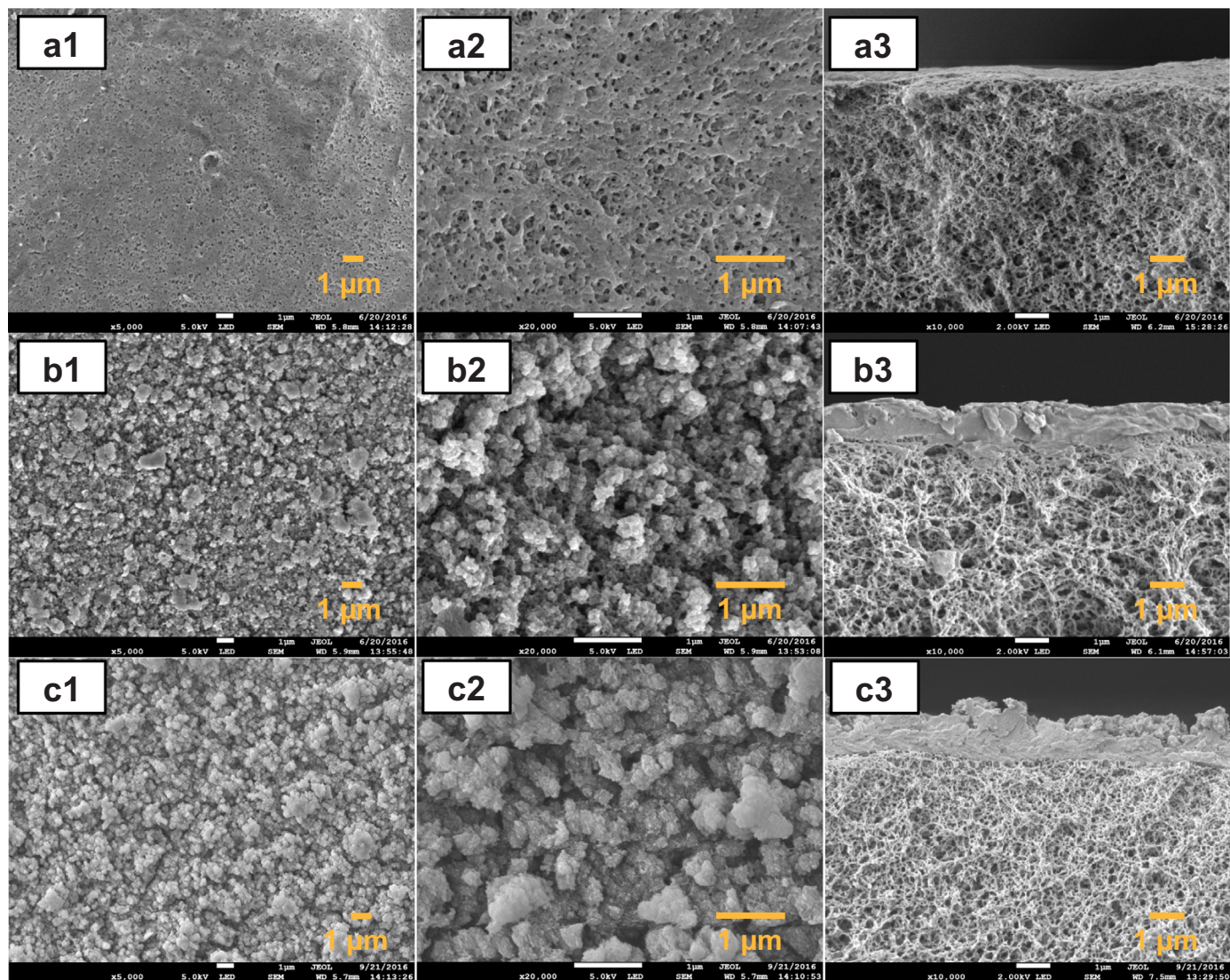


Fig. 2. FESEM images of the outer surface morphologies of the pristine PVDF (a1 and a2), PVDF-P (b1 and b2), and ultrasonicated PVDF-P (c1 and c2) membranes; FESEM images of the cross-section morphologies of the pristine PVDF (a3), PVDF-P (b3), and ultrasonicated PVDF-P (c3) membranes.

The overflow from the permeate reservoir was collected into a tank placed on a weighing balance to determine the temporal changes in mass with an accuracy of  $\pm 0.1$  g. The temporal changes in permeate conductivity were recorded to an accuracy of  $\pm 0.1 \mu\text{S cm}^{-1}$ . Most importantly, all tubes and membrane modules used in the experimental rig were insulated with insulation foam to minimize heat loss during the process.

### 3. Results and discussion

#### 3.1. Membrane surface characterizations

Fig. 2 shows the outer surface and cross-section morphologies of the pristine PVDF and PVDF-P membranes. It was evident from these images that the changes in surface morphology of the pristine PVDF membrane after modification were rather radical. As shown in Fig. 2(a1) and (a2), the pristine PVDF membrane surface had abundant pores. The co-deposition of PDA/PEI formed agglomerates on the membrane surface that thoroughly covered the surface and blocked membrane pores (shown in Fig. 2(b1) and (b2)). These deposited agglomerates created a hierarchical structure with a higher roughness, which was attested by the surface roughness parameters presented in Table 2. According to the Wenzel model, roughness plays a critical role in enhancing surface intrinsic wetting ability [59], which will be further discussed in Section 3.3. Fig. 2(b3) suggests that the thickness of the grafted layer was around  $1 \mu\text{m}$  and did not penetrate into the bulk of the pristine PVDF substrate. The stability of the grafted layer on the membrane surface was assessed by subjecting the PVDF-P membrane to bath sonication. The FESEM images of the outer surface and cross-section morphologies of the PVDF-P membrane after ultrasonication are shown in Fig. 2(c1)–(c3). The result shows that the grafted layer remained intact and minimal changes to the surface morphology were observed. The FESEM images were indicative of the robust structural stability of the PVDF-P membrane under harsh conditions.

The distinct difference in pore size distribution between the pristine PVDF and PVDF-P membranes suggests that the co-deposition of PDA/PEI altered the structural property of the pristine PVDF membrane. From Fig. A1, it can be observed that the pristine PVDF membrane had a well-defined bimodal distribution with a mean pore size of  $0.027 \mu\text{m}$ . On the other hand, the PVDF-P membrane had a much narrower pore size distribution with a smaller mean pore size of  $0.017 \mu\text{m}$ , which is in agreement with the FESEM images. The co-deposition of PDA/PEI would have effectively covered most of the pores on the outer surface of the PVDF-P membrane and caused a reduction in its pore size. As such, it is expected that the PVDF-P membrane would be less vulnerable to pore wetting due to the additional protection provided by the grafted layer [4].

#### 3.2. Deposition of PDA/PEI on the PVDF-P membrane surface

In Fig. 3, the ATR-FTIR spectra provided an evidence on the co-deposition of PDA/PEI on the PVDF-P membrane surface as shown by the presence of two noticeable absorption peaks at  $1541 \text{ cm}^{-1}$  and

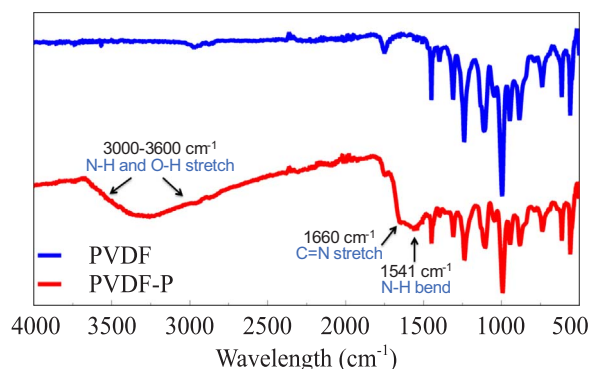


Fig. 3. ATR-FTIR spectra of the outer surfaces of the pristine PVDF and PVDF-P membranes. Transmittance was normalized against the CF peak.

$1660 \text{ cm}^{-1}$ , which were attributed to the N-H bending in PDA and C=N stretching within the PDA/PEI cross-links, respectively [41]. Besides that, the broad peak observed between  $3000$  and  $3600 \text{ cm}^{-1}$  on the PVDF-P membrane surface could be attributed to the N-H stretching and O-H stretching in the amine- and hydroxyl-functional groups found on its surface [53,60].

In order to further understand the elemental composition and chemical state of the PDA/PEI grafting layer, XPS analyses were carried out. The survey scan spectra of the pristine PVDF and PVDF-P membranes along with the deconvolution spectra of the PVDF-P membrane outer surface are presented in Fig. 4 while the surface elemental compositions of both the pristine PVDF and PVDF-P membranes are summarized in Table 3. The inner surface elemental compositions of both the pristine PVDF and PVDF-P membranes were similar, which proves that there was no penetration of the hydrophilic grafting solution through the hydrophobic pores of the PVDF substrate. As shown in Fig. 4(a), the disappearance of the F 1s and Cl 2p peaks along with the appearance of N 1s peak on the outer surface of the PVDF-P membrane suggested the successful co-deposition of PDA/PEI and its complete coverage on the membrane surface. As listed in Table 3, the C 1s and O 1s concentrations of the PVDF-P membrane outer surface were increased after modification and the N/O ratio reached 0.9, which was close to the value reported by Yang et al. [41]. As shown in the deconvoluted spectra of the PVDF-P membrane in Fig. 4(b)–(d), the C 1s core-level spectrum could be curve-fitted with three peak components at binding energies (BE) of 284.8 eV, 285.9 eV, and 287.5 eV, which corresponded to the C-C/C-H, C-O/C-N, and C=O bonds, respectively. The N 1s core-level spectrum was curve-fitted with two peak components, one at a BE of 399.8 eV for the C-N bond and the other at a BE of 402.0 eV for the protonated amine-functional group. The O 1s core-level spectrum was also curve-fitted with two peak components at BE of 531.2 eV and 532.6 eV, which were assigned to the C=O and C-O bonds groups, respectively. The XPS analysis results were supportive of the following proposed PDA reaction mechanisms with PEI.

The oxidative self-polymerization of dopamine involves its catechol group autoxidizing to form dopamine quinone [61], which in turn follows several reaction pathways to form PDA [62–67]. The primary amine-functional groups on PEI may react with dopamine quinones to form Michael-type adducts or Schiff bases through Michael addition or Schiff base reaction, respectively, as illustrated in Fig. 5. Thus, the incorporation of PEI can form covalent cross-linking with PDA due to the reaction among catechol and amino groups [41].

The surface charge properties of the pristine PVDF and PVDF-P membranes were studied using the streaming potential measurement at a pH range of 3–10 and the results are shown in Fig. 6. Throughout the entire tested pH range, the pristine PVDF membrane was mostly negatively charged. The co-deposition of PDA/PEI slightly neutralized the negative charge on the PVDF membrane surface, resulting in a right shift of the zeta potential curve. The isoelectric point of the PVDF-P

Table 2

Surface roughness parameters and water contact angles of the pristine PVDF and PVDF-P membranes.

Membranes	Roughness			Water contact angle (°)
	$R_a^a$ (nm)	$R_q^b$ (nm)	$R_z^c$ (nm)	
PVDF	25.6	31.9	258.3	$109.5 \pm 1.2$
PVDF-P	197.0	243.1	1689.2	$25.7 \pm 4.0$

<sup>a</sup> Average roughness.

<sup>b</sup> Root-mean-squared roughness.

<sup>c</sup> Ten point average roughness.

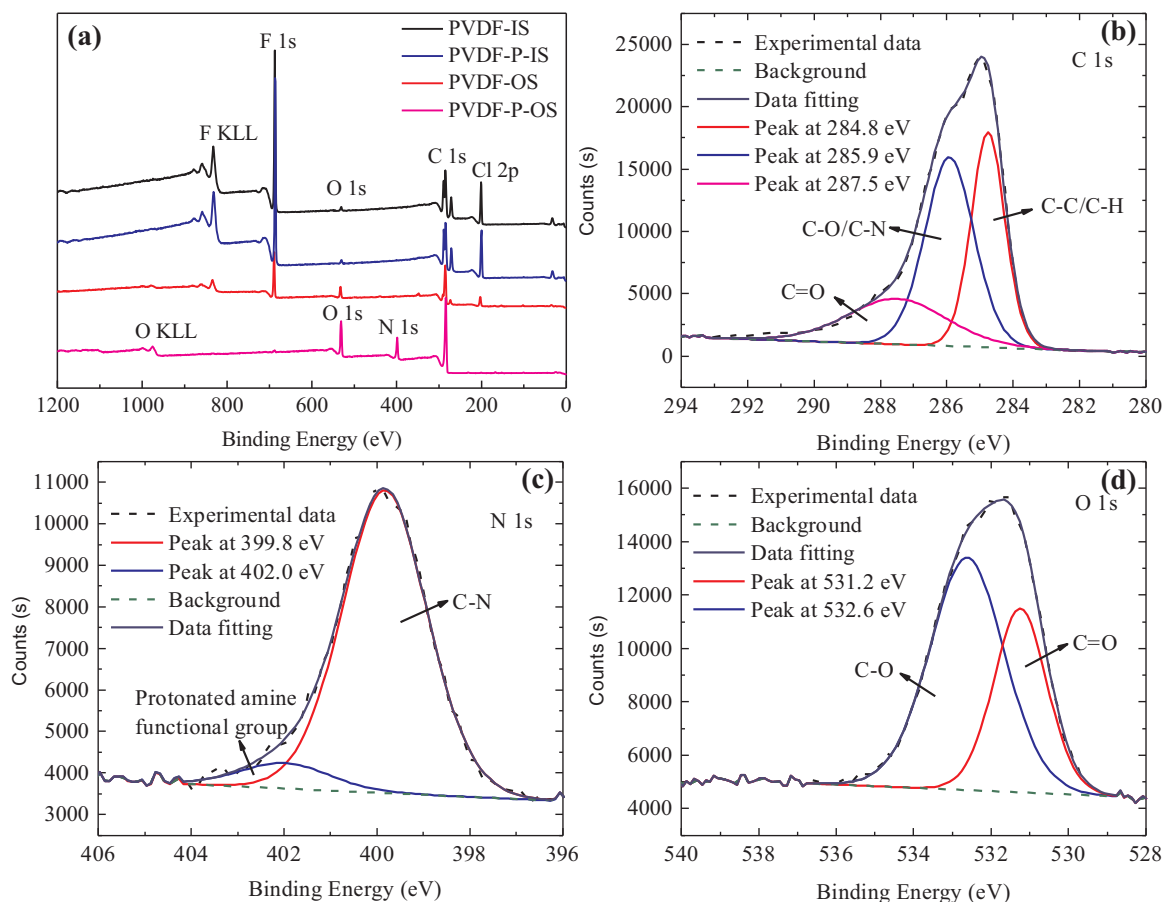


Fig. 4. (a) XPS survey scan spectra of the inner (IS) and outer (OS) surfaces of the pristine PVDF and PVDF-P membranes. Deconvolution of (b) C 1s, (c) N 1s, and (d) O 1s spectra of the outer surface of the PVDF-P membrane.

Table 3

The elemental compositions (in atomic percentage) of the inner (IS) and outer (OS) surfaces of the pristine PVDF and PVDF-P membranes.

Membrane	O 1s (at%)	C 1s (at%)	F 1s (at%)	Cl 2p (at%)	N 1s (at%)
PVDF-IS	1.21	56.85	28.81	13.31	–
PVDF-P-IS	0.96	54.43	31.23	13.37	–
PVDF-OS	6.55	71.63	15.60	6.22	–
PVDF-P-OS	12.63	75.80	0.35	0.20	11.02

membrane was 3.8.

### 3.3. Wetting properties of the pristine and modified membranes

As listed in Table 2, the pristine PVDF and PVDF-P membranes had water contact angles of  $109.5 \pm 1.2^\circ$  and  $25.7 \pm 4.0^\circ$ , respectively. This suggests that the pristine PVDF membrane underwent transition from being hydrophobic to hydrophilic after surface modification. The presence of polar amine- and hydroxyl-functional groups of PDA/PEI imparted hydrophilicity to the PVDF-P membrane surface. In addition, the hierarchical surface structure further enhanced the hydrophilic effects [59]. In order to investigate on the intrinsic wetting properties of the membranes in the presence of oil droplets, the underwater captive bubble method was employed. The video clips (Videos S1 and S2) showing the interaction of the oil droplet with the pristine PVDF and PVDF-P membrane surfaces are provided as Supplementary materials. The relevant captured images of the interactions are depicted in Fig. 7. It was evident that the pristine PVDF membrane surface was underwater oleophobic, which was instantaneously wetted by the oil droplet upon contact. The oil contact angle approached  $0^\circ$  within 15 s. On the

other hand, the PVDF-P membrane surface exhibited underwater superoleophobicity. The oil droplet would not leave the needle and stick onto the membrane surface even after several attempts. The oil droplet remained spherical in shape and no apparent deformation was observed. The underwater superoleophobicity of the PVDF-P membrane could be explained from the thermodynamically favorable interaction between its surface hydrophilic groups and surrounding water molecules. The hydrophilic moieties on the grafted layer could interact strongly with surrounding water molecules and other polar molecules to form hydrogen bonds, which resulted in an interfacial hydration layer. This hydrogen-bonded hydration layer provided a significant energetic barrier for the oil droplets to overcome in order to be attached onto the PVDF-P membrane surface. This suggests that the PVDF-P membrane had an oil-adhesion resistant surface and could possibly be anti-fouling when used for treating O/W emulsions.

Supplementary material related to this article can be found online at <http://dx.doi.org/10.1016/j.memsci.2017.06.089>.

### 3.4. Membrane performance in DCMD tests

#### 3.4.1. Saline feeds with four types of surfactant

To ascertain that the PDA/PEI grafted layer did not affect the intrinsic MD performance of the PVDF-P membrane, a baseline test was first conducted by using 3.5 wt% NaCl feed solution and the results are shown in Fig. 8. It can be observed that the permeate flux of the PVDF-P membrane was comparable to that of the pristine PVDF membrane throughout the operation, which suggests that the grafted layer did not provide additional resistance to vapor transport through the hydrophobic pores. As observed in the outer surface morphology of the PVDF-P membrane (Fig. 2(b1) and (b2)), there were micro-channels within

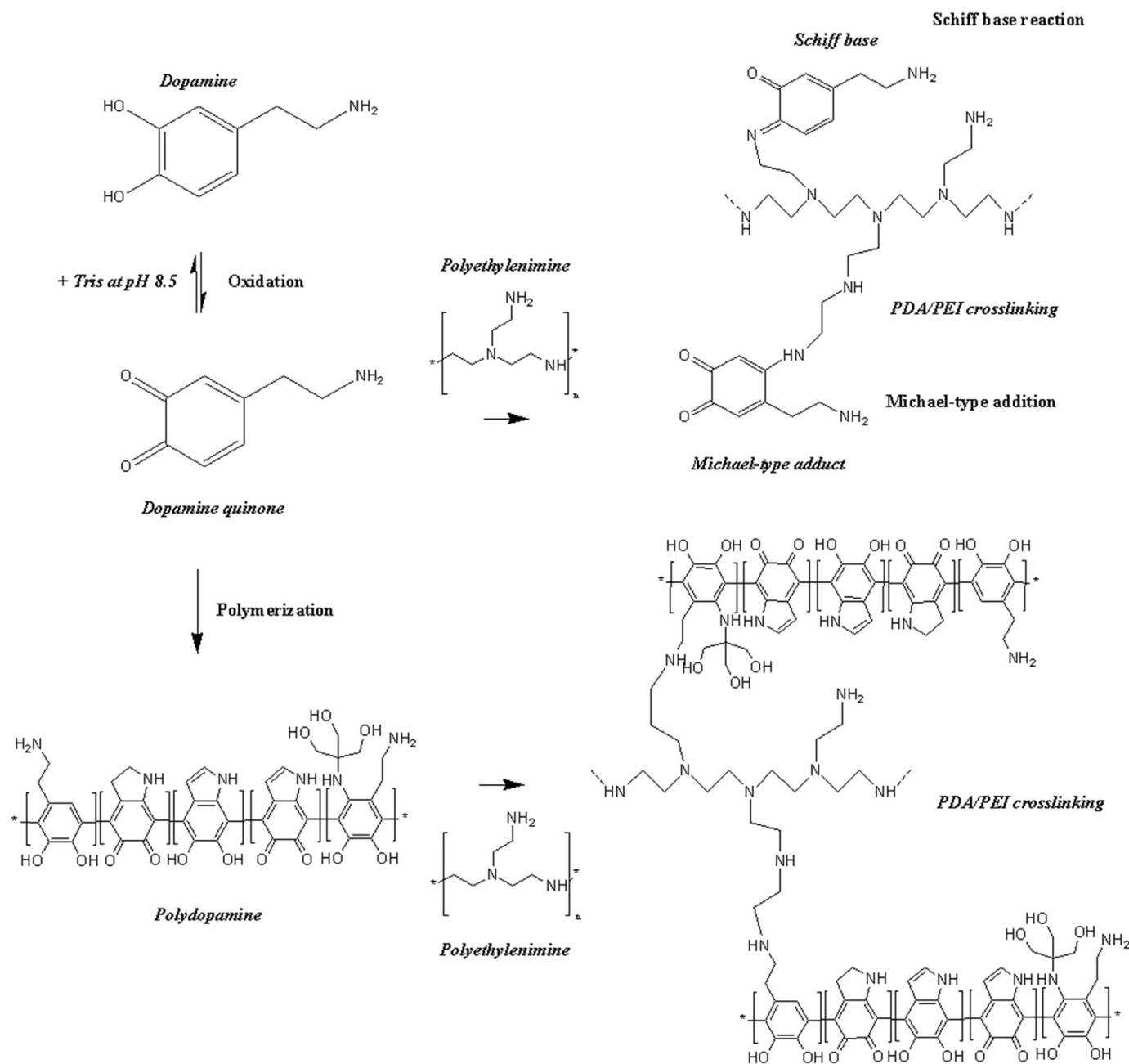


Fig. 5. Proposed polydopamine reaction mechanisms with polyethylenimine.

the hierarchical structure formed by the PDA/PEI asperities. These micro-channels allowed water molecules to flow through the hydrophilic grafted layer. Even though the pore size of the PVDF-P membrane outer surface became smaller after functional group modification, the compromise between smaller membrane pores and a hydrophilic surface ensured a comparable flux for the PVDF-P membrane. Similar to the pristine PVDF membrane, no wetting was observed for the PVDF-P membrane after 24 h of operation. This vindicates that only the shell side of the PVDF-P membrane was coated with a hydrophilic layer and as such, the substrate pores remained hydrophobic for the vapor transport while rejecting the non-volatile NaCl solute.

After the baseline test, DCMD experiments were performed on both the pristine PVDF and PVDF-P membranes by feeding  $50 \text{ mg L}^{-1}$  of non-ionic (Span<sup>®</sup> 20 and Tween<sup>®</sup> 20), anionic (SDS), and cationic (DTAB) surfactants. High salinity wastewater, such as oilfield or shale gas produced water, often contains surfactants that reduce its surface tension significantly and in turn poses a challenge to MD membranes.

To ensure a fair comparison, surfactants with a 12-carbon hydrophobic tail were selected. The hydrophilic-lipophilic balance (HLB) values of these surfactants and surface tensions of the respective solutions are provided in Table 1. HLB is an empirical value that defines the relationship of the polar and non-polar groups of a surfactant. The lower the HLB value, the more hydrophobic (oil-soluble) the surfactant is. The significantly different wetting and fouling behaviors of these two membranes are illustrated in Fig. 9. In the case of Span<sup>®</sup> 20 (Fig. 9(a)), the pristine PVDF membrane experienced severe wetting and fouling, as indicated by the rapidly increased permeate conductivity and declined water flux. In comparison, the PVDF-P membrane showed more stable MD performance, where neither fouling nor wetting was observed after 80 h of operation. The permeate of the PVDF-P membrane was of excellent quality, with its conductivity remaining stable at  $3.5 \mu\text{S cm}^{-1}$  throughout the operation. The stark contrast in the performances of the pristine PVDF and PVDF-P membranes was believed to be due to their different surface hierarchical structures and opposing wetting

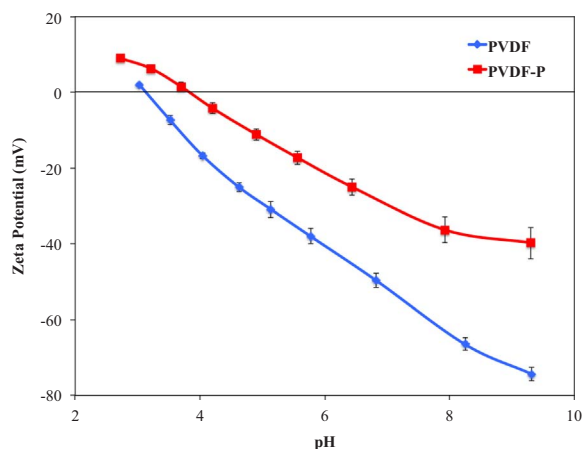


Fig. 6. Surface zeta potentials of the pristine PVDF and PVDF-P membranes as a function of pH. 1 mM NaCl was used as the electrolyte solution.

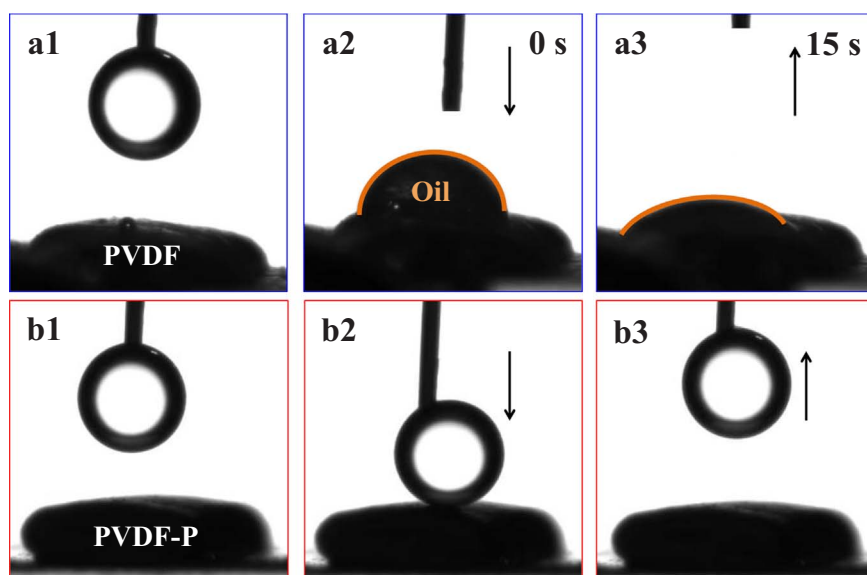


Fig. 7. Captured images of the underwater interactions between oil droplets tethered via a needle and the pristine PVDF (a1-a3) and PVDF-P (b1-b3) membrane surfaces.

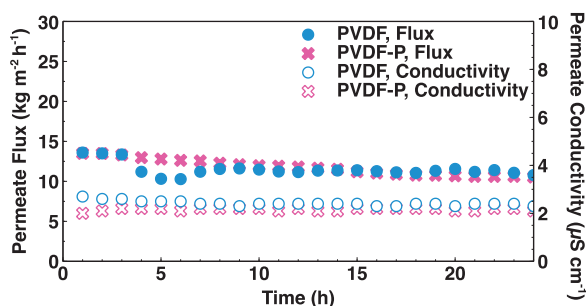


Fig. 8. DCMDC performances of the pristine PVDF and PVDF-P membranes by feeding 3.5 wt% NaCl. (Feed volumetric flow rate ( $Q_f$ ) = 0.7 L min<sup>-1</sup>; Permeate volumetric flow rate ( $Q_p$ ) = 0.25 L min<sup>-1</sup>; Feed temperature ( $T_f$ ) = 333 K; Permeate temperature ( $T_p$ ) = 293 K).

properties. As discussed in our previous study [68], Span<sup>®</sup> 20 is a relatively hydrophobic surfactant with a low HLB value of 8.6. As such, the Span<sup>®</sup> 20 unimers have the tendency to adsorb onto hydrophobic surfaces to form a monolayer via hydrophobic interactions [69]. For the pristine PVDF membrane, the drastic water flux decline and permeate conductivity increase were due to the adsorption of Span<sup>®</sup> 20 unimers onto its hydrophobic membrane surface and pores, which resulted in complete pore blockage and severe pore wetting [68]. In comparison, the hydrophilic coating on the PVDF-P membrane surface avoided such

hydrophobic interactions. The hydrophilic moieties on the PVDF-P membrane surface strongly interacted with water to form a hydration layer on its surface, which in turn prevented the hydrophobic tails of surfactants from attaching. Such an anti-fouling mechanism is supported by its underwater superoleophobicity as suggested by the captive bubble measurement. Similar phenomenon was also observed in the case of Tween<sup>®</sup> 20 as feed, in which a very stable permeate flux was achieved for the PVDF-P membrane after 115 h of operation while the permeate conductivity remained relatively low at 20  $\mu\text{S cm}^{-1}$  (Fig. 9(b)). The greatly improved anti-fouling and anti-wetting properties of the PVDF-P membrane make it robust for water recovery from low surface tension feeds containing non-ionic surfactant unimers such as Span<sup>®</sup> 20 and Tween<sup>®</sup> 20 by MD.

As shown in Fig. 9(c), the PVDF-P membrane experienced no wetting after 90 h of operation when 50 mg L<sup>-1</sup> of SDS was used as feed. Its final permeate conductivity was only 3.5  $\mu\text{S cm}^{-1}$  as compared to 5660  $\mu\text{S cm}^{-1}$  in the case of the pristine PVDF membrane. However, membrane fouling was observed on both the pristine PVDF and PVDF-P

membranes as indicated by the flux decline. The fouling mechanisms for these two membranes were different, which will be discussed below. Different from non-ionic surfactants, both the hydrophobic and electrostatic interactions play crucial roles in the adsorption of ionic surfactants. In the case of the pristine PVDF membrane, its negatively charged surface could repel the similarly charged SDS unimers. However, this was offset by the dominant hydrophobic interactions between the hydrophobic tails of the SDS unimers and the hydrophobic PVDF membrane surface. Such hydrophobic interactions resulted in the adsorption of some SDS unimers, as represented by the flux decline after approximately 12 h of operation. The fouling extent caused by SDS was not as severe as that from Span<sup>®</sup> 20 and this was due to its relatively hydrophilic nature, which commensurate with its higher HLB value [70]. Like the other surfactants, the adsorption of surface active agent SDS also resulted in pore wetting as represented by the increase in permeate flux and permeate conductivity towards the end of the operation. On the other hand, the hydrophilic PDA/PEI grafting layer on the PVDF-P membrane surface could alleviate the hydrophobic interactions while the electrostatic interactions were the dominant factor for membrane fouling. In theory, the negatively charged PVDF-P membrane surface should have repelled the negatively charged SDS unimers in the solution at around pH 7. However, the electrostatic attraction between the protonated amine-functional groups on the PVDF-P membrane surface and the sulfate groups present in the hydrophilic heads of the SDS unimers resulted in membrane fouling [71,72].



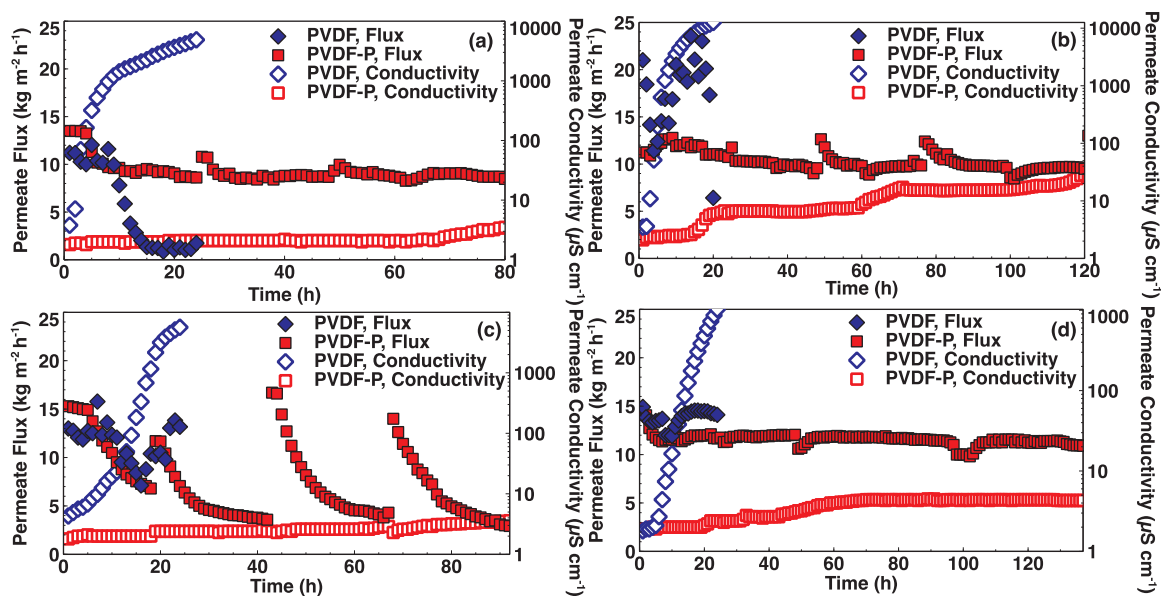


Fig. 9. DCMD performances of the pristine PVDF and PVDF-P membranes by feeding 50 mg L<sup>-1</sup> of (a) Span<sup>®</sup> 20, (b) Tween<sup>®</sup> 20, (c) SDS, and (d) DTAB in 3.5 wt% NaCl. For the SDS experiment, PVDF-P membrane was flushed with Milli-Q<sup>®</sup> water when flux reached the lowest point. For each experiment, the feed tank was periodically refilled with overflow from the permeate reservoir to maintain the feed concentration. ( $Q_f = 0.7 \text{ L min}^{-1}$ ;  $Q_p = 0.25 \text{ L min}^{-1}$ ;  $T_f = 333 \text{ K}$ ;  $T_p = 293 \text{ K}$ ).

Fortunately, this fouling was reversible. The permeate flux of the PVDF-P membrane was able to return to its initial level by cleaning it repeatedly with Milli-Q<sup>®</sup> water, as shown in Fig. 9(c). The PVDF-P membrane remained anti-wetting despite the electrostatic adsorption of the SDS unimers because the grafted PDA/PEI layer protected the mouth of the membrane pores, which in turn could maintain the LEP of these pores.

In contrast to anionic surfactant SDS, the PVDF-P membrane did not experience any fouling or wetting after 137 h of operation when feeding 50 mg L<sup>-1</sup> of cationic surfactant DTAB (Fig. 9(d)). Its permeate flux was stable while the permeate quality was excellent throughout the operation, achieving a final electrical conductivity of 4.3 μS cm<sup>-1</sup>. Its anti-fouling performance could be explained by the presence of the hydration layer and electrostatic repulsive forces between the positively charged quaternary ammonium heads of the DTAB unimers and the protonated amine-functional groups present in the grafted layer. In contrast, the lack of positive functional groups on the negatively charged surface of the pristine PVDF membrane would attract some DTAB unimers due to both hydrophobic and electrostatic interactions, leading to wetting of the membrane pores. It recorded a final permeate conductivity of 1026 μS cm<sup>-1</sup> after 24 h of operation. From the above discussions, it could be inferred that the presence of protonated amine-functional groups on the outer surface of the PVDF-P membrane was effective in preventing the adsorption of cationic surfactants.

### 3.4.2. Surfactant-stabilized petroleum-in-water emulsions

After the DCMD experiments with various surfactants, the fouling and wetting behaviors of the pristine PVDF and PVDF-P membranes were further evaluated by feeding 500 mg L<sup>-1</sup> of surfactant-stabilized petroleum-in-water emulsion. The O/W emulsion was made kinetically stable by adding the surfactant DTAB in order to keep its oil droplet size below 10 μm [69]. The mean oil droplet size was 2.43 μm, which was much bigger than the nominal pore sizes of the pristine PVDF and PVDF-P membranes and was likely to cause pore blockage on the respective membrane surfaces. The pH and corresponding zeta potential of the DTAB-stabilized petroleum-in-water emulsion were measured to be 5.7 and 22.9 ± 1.4 mV, respectively.

As presented in Fig. 10, the PVDF-P membrane showed robust long-term MD performance, maintaining a stable flux for up to a week of operation with a final permeate conductivity of 5.5 μS cm<sup>-1</sup>. It was

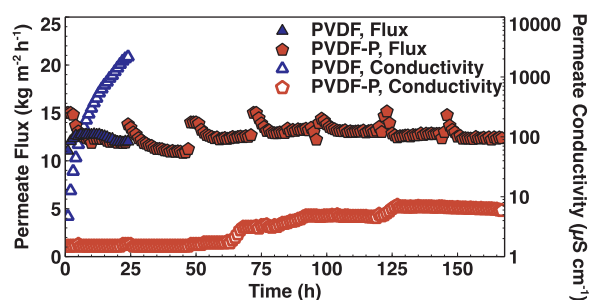


Fig. 10. DCMD performances of the pristine PVDF and PVDF-P membranes by feeding 500 mg L<sup>-1</sup> of DTAB-stabilized petroleum-in-water emulsion. Fresh emulsions were prepared every 24 h for the PVDF-P experiment. ( $Q_f = 0.7 \text{ L min}^{-1}$ ;  $Q_p = 0.25 \text{ L min}^{-1}$ ;  $T_f = 333 \text{ K}$ ;  $T_p = 293 \text{ K}$ ).

hypothesized that its anti-fouling and anti-wetting properties were ascribed to the tightly bounded hydration layer on its hydrophilic outer surface as illustrated in Fig. 11 [73]. When the O/W emulsion came into contact with the PVDF-P membrane surface, the hydrophilic moieties could interact strongly with water molecules to form a hydrogen-bonded network within the hierarchical structure of the grafted layer. This strong surface hydration layer provided a significant energetic barrier for the oil droplets to overcome in order to be adsorbed onto the PVDF-P membrane interface. Oil-adhesion on the membrane surface is only possible when the water molecules are expelled from the hierarchical structure, which is usually caused by dehydration. Dehydration leads to the unfavorable decrease in entropy, which in turn reduces the energetic barrier and facilitates membrane fouling [74]. Also, the electrostatic repulsive forces that existed between the positively charged O/W emulsion and protonated amine-functional groups on the PVDF-P membrane surface made it difficult for the attachment of oil droplets. In other words, the strongly hydrogen-bonded hydration layer coupled with the electrostatic repulsion interactions rendered the PVDF-P membrane surface to be oil-adhesion resistant. In contrast, the lack of such a protection layer on the pristine PVDF membrane surface made it susceptible to oil-adhesion and pore wetting. Both the hydrophobic interactions (between the hydrophobic membrane surface and oil droplets) and electrostatic attractive forces (between the negatively charged membrane surface and positively charged O/W emulsion) made it easier for the attachment and accumulation of oil droplets on

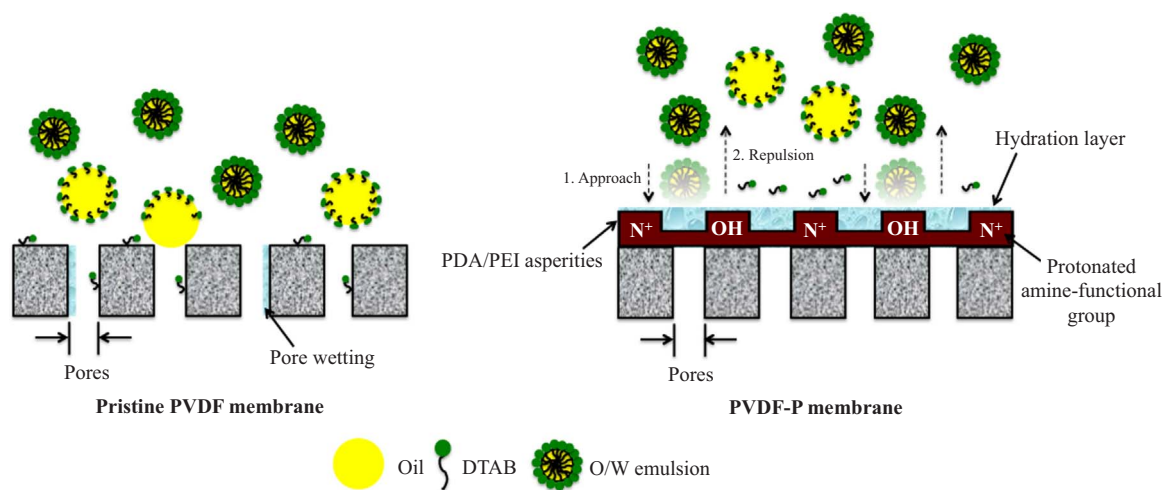


Fig. 11. Schematic of interaction of DTAB-stabilized O/W emulsion with the pristine PVDF and PVDF-P membranes.

the pristine PVDF membrane surface. To put it succinctly, the anti-fouling and anti-wetting abilities of MD membranes could be achieved through the efficacious combinative effects of surface hydration and electrostatic repulsion.

### 3.5. Comparisons to other MD membranes

Table 4 summarizes the DCMD performance of the PVDF-P membrane for various feed solutions along with other MD membranes from literature. It can be seen that the PVDF-P membrane exhibits robust long-term performance with stable flux and excellent permeate quality (permeate conductivities were less than  $5.5 \mu\text{S cm}^{-1}$  and salt rejection rates were above 99.9%) by feeding high concentration surfactant solutions and O/W emulsions for up to one week of operation. This is superior to all other previously reported MD membranes. For example, compared with the  $\text{SiO}_2$ -incorporated PVDF membrane [28], the PVDF-P membrane reported in this work delivered better anti-fouling and anti-wetting performances by feeding surfactants of 5 times the concentration. The study conducted by Wang et al. reported salt rejections instead of final permeate conductivity values [27,29]. However, the final permeate conductivity values are better representations of the permeate quality in MD operations. The robustness of the PVDF-P membrane suggests its potential for water recovery from low surface tension feeds such as produced water via the DCMD process.

## 4. Conclusions

A composite PVDF membrane with in-air hydrophilic/underwater superoleophobic properties was fabricated via a facile method through single-step co-deposition of PDA/PEI onto a hydrophobic PVDF

substrate. The fouling and wetting behaviors of the pristine PVDF and modified PVDF membranes were systematically studied via DCMD experiments by feeding amphiphilic surfactants and O/W emulsion. The results reveal that the modified PVDF membrane exhibited excellent anti-wetting properties regardless of the type of surfactant. In addition, it exhibited excellent anti-fouling properties against both non-ionic and cationic surfactants. More importantly, the modified membrane showed very promising stability (one week of operation) in the recovery of water from DTAB-stabilized petroleum-in-water emulsion without experiencing fouling and wetting. The robust MD performance was possible because of the following two reasons. Firstly, an interfacial hydration layer was formed within the hierarchical structure of the hydrophilic grafting layer, which prevented the attachment of oil droplets. Secondly, the protonated amine-functional groups on the membrane outer surface were able to repel the positively charged O/W emulsion. Interestingly, the thin grafting layer did not impede on the permeate flux of the modified membrane and instead protected the membrane pores from oil adsorption. This study suggests that the underwater superoleophobic mussel-inspired modified PVDF membrane could potentially be used for highly effective and environmentally friendly water recovery from low surface tension solutions such as produced water via DCMD.

## Acknowledgements

This work was funded by the Johnson Matthey Technology Centre. The authors would also like to acknowledge funding support from the Singapore Economic Development Board to the Singapore Membrane Technology Centre.

Table 4

Comparison of performances among various MD membranes.

Membrane	Feed	Test duration (h)	$C_{p,final}$ ( $\mu\text{S cm}^{-1}$ )	Salt rejection (%)	Reference
PVDF-P	50 mg L <sup>-1</sup> Span® 20	80	3.5	99.99	Current work
PVDF-P	50 mg L <sup>-1</sup> Tween® 20	115	20	99.96	Current work
PVDF-P	50 mg L <sup>-1</sup> SDS	90	3.5	99.99	Current work
PVDF-P	50 mg L <sup>-1</sup> DTAB	137	4.3	99.99	Current work
PVDF-P	500 mg L <sup>-1</sup> DTAB/Oil	168	5.5	99.99	Current work
$\text{SiO}_2$ /PVDF	10 mg L <sup>-1</sup> SDBS <sup>a</sup>	104	~ 80	99.9	[28]
$\text{SiO}_2$ /PVDF	10 mg L <sup>-1</sup> kerosene	200	~ 100	99.8	[28]
SiNPs/PVDF	1000 mg L <sup>-1</sup> crude oil	36	N.A. <sup>b</sup>	~ 100	[27]
PDA/SiNPs/PVDF	1000 mg L <sup>-1</sup> crude oil	12	N.A. <sup>b</sup>	99.9	[29]

<sup>a</sup> Sodium dodecyl benzene sulfonate.

<sup>b</sup> Not applicable. The final permeate conductivity values of these experiments were not provided.

## Appendix A. Pore size distributions of the pristine PVDF and PVDF-P membranes

See Fig. A1.

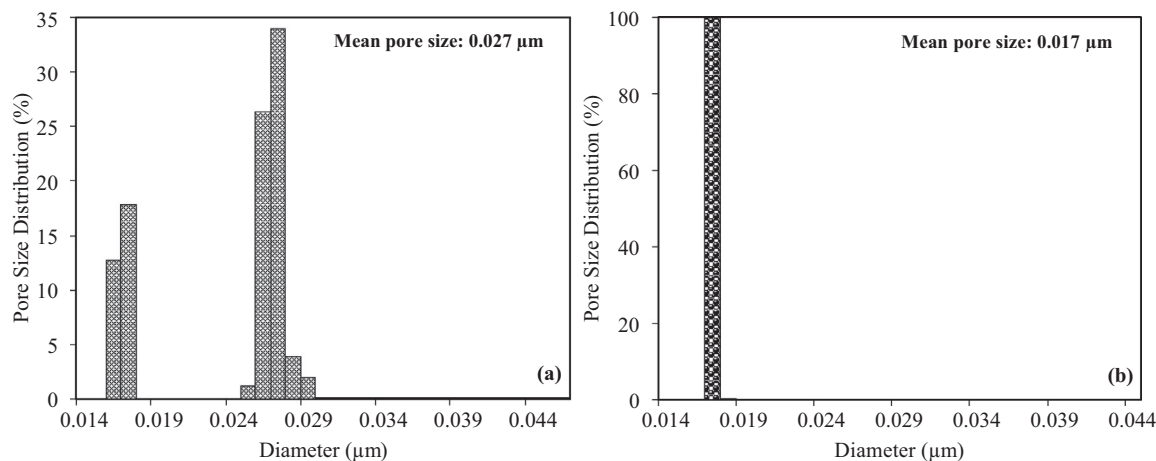


Fig. A1. Pore size distributions of the (a) pristine PVDF and (b) PVDF-P membranes.

## References

- [1] IEA, Key World Energy Statistics 2016, 2016.
- [2] A. Fakhru'l-Razi, A. Pendashteh, L.C. Abdullah, D.R.A. Biak, S.S. Madaeni, Z.Z. Abidin, Review of technologies for oil and gas produced water treatment, *J. Hazard. Mater.* 170 (2–3) (2009) 530–551.
- [3] L. Toop, Produced water treatment trends move towards reuse, in *Oil and Gas Product News*, Dow, 2016.
- [4] X. Yang, R. Wang, L. Shi, A.G. Fane, M. Debowski, Performance improvement of PVDF hollow fiber-based membrane distillation process, *J. Membr. Sci.* 369 (1–2) (2011) 437–447.
- [5] G. Chen, X. Yang, Y. Lu, R. Wang, A.G. Fane, Heat transfer intensification and scaling mitigation in bubbling-enhanced membrane distillation for brine concentration, *J. Membr. Sci.* 470 (2014) 60–69.
- [6] Y. Liao, R. Wang, M. Tian, C. Qiu, A.G. Fane, Fabrication of polyvinylidene fluoride (PVDF) nanofiber membranes by electro-spinning for direct contact membrane distillation, *J. Membr. Sci.* 425–426 (2013) 30–39.
- [7] M. Safavi, T. Mohammadi, High-salinity water desalination using VMD, *Chem. Eng. J.* 149 (1–3) (2009) 191–195.
- [8] A. Alkudhri, N. Darwish, N. Hilal, Treatment of high salinity solutions: application of air gap membrane distillation, *Desalination* 287 (2012) 55–60.
- [9] A.F. Janson, S. Adham, F. Benyahia, R. Dores, A. Husain, J. Minier-Matar, Membrane distillation of high salinity brines using low grade waste heat, in: *Proceedings of the AMTA/AWWA Membrane Technology Conference and Exposition 2013*, February 25, 2013 – February 28, 2013. San Antonio, TX, United States, American Water Works Association, 2013.
- [10] Y.M. Manawi, M.A.M.M. Khraishah, A.K. Fard, F. Benyahia, S. Adham, A predictive model for the assessment of the temperature polarization effect in direct contact membrane distillation desalination of high salinity feed, *Desalination* 341 (1) (2014) 38–49.
- [11] J. Li, Y. Guan, F. Cheng, Y. Liu, Treatment of high salinity brines by direct contact membrane distillation: effect of membrane characteristics and salinity, *Chemosphere* 140 (2015) 143–149.
- [12] N. Dow, S. Gray, J.-D. Li, J. Zhang, E. Ostarcevic, A. Liubinas, P. Atherton, G. Roeszler, A. Gibbs, M. Duke, Pilot trial of membrane distillation driven by low grade waste heat: membrane fouling and energy assessment, *Desalination* 391 (2016) 30–42.
- [13] R. Schwantes, A. Cipollina, F. Gross, J. Koschikowski, D. Pfeifle, M. Rolletschek, V. Subiela, Membrane distillation: solar and waste heat driven demonstration plants for desalination, *Desalination* 323 (2013) 93–106.
- [14] A.E. Jansen, J.W. Assink, J.H. Hanemaaijer, J. van Medevoort, E. van Sonsbeek, Development and pilot testing of full-scale membrane distillation modules for deployment of waste heat, *Desalination* 323 (2013) 55–65.
- [15] H.C. Duong, P. Cooper, B. Nelemans, T.Y. Cath, L.D. Nghiem, Evaluating energy consumption of air gap membrane distillation for seawater desalination at pilot scale level, *Sep. Purif. Technol.* 166 (2016) 55–62.
- [16] M. Gryta, J. Grzechulska-Damszel, A. Markowska, K. Karakulski, The influence of polypropylene degradation on the membrane wettability during membrane distillation, *J. Membr. Sci.* 326 (2) (2009) 493–502.
- [17] Y. Liao, R. Wang, A.G. Fane, Engineering superhydrophobic surface on poly(vinylidene fluoride) nanofiber membranes for direct contact membrane distillation, *J. Membr. Sci.* 440 (2013) 77–87.
- [18] Y. Liao, C.-H. Loh, R. Wang, A.G. Fane, Electrospun superhydrophobic membranes with unique structures for membrane distillation, *ACS Appl. Mater. Interfaces* 6 (18) (2014) 16035–16048.
- [19] Y. Liao, R. Wang, A.G. Fane, Fabrication of bioinspired composite nanofiber membranes with robust superhydrophobicity for direct contact membrane distillation, *Environ. Sci. Technol.* 48 (11) (2014) 6335–6341.
- [20] A. Razmjou, E. Arifin, G. Dong, J. Mansouri, V. Chen, Superhydrophobic modification of TiO<sub>2</sub> nanocomposite PVDF membranes for applications in membrane distillation, *J. Membr. Sci.* 415–416 (2012) 850–863.
- [21] M. Suwan, Y. Yun, J. Mansouri, V. Chen, Fouling and crystallisation behaviour of superhydrophobic nano-composite PVDF membranes in direct contact membrane distillation, *J. Membr. Sci.* 463 (2014) 102–112.
- [22] C. Boo, J. Lee, M. Elimelech, Engineering surface energy and nanostructure of microporous films for expanded membrane distillation applications, *Environ. Sci. Technol.* 50 (15) (2016) 8112–8119.
- [23] X. Liu, J. Gao, Z. Xue, L. Chen, L. Lin, L. Jiang, S. Wang, Bioinspired oil strider floating at the oil/water interface supported by huge superoleophobic force, *ACS Nano* 6 (6) (2012) 5614–5620.
- [24] J. Yong, F. Chen, Q. Yang, D. Zhang, U. Farooq, G. Du, X. Hou, Bioinspired underwater superoleophobic surface with ultralow oil-adhesion achieved by femto-second laser microfabrication, *J. Mater. Chem. A* 2 (23) (2014) 8790–8795.
- [25] J. Yong, F. Chen, Q. Yang, G. Du, C. Shan, H. Bian, U. Farooq, X. Hou, Bioinspired transparent underwater superoleophobic and anti-oil surfaces, *J. Mater. Chem. A* 3 (18) (2015) 9379–9384.
- [26] W. Liu, X. Liu, J. Fangteng, S. Wang, L. Fang, H. Shen, S. Xiang, H. Sun, B. Yang, Bioinspired polyethylene terephthalate nanocone arrays with underwater superoleophobicity and anti-bioadhesion properties, *Nanoscale* 6 (22) (2014) 546–554.
- [27] Z. Wang, D. Hou, S. Lin, Composite membrane with underwater-oleophobic surface for anti-oil-fouling membrane distillation, *Environ. Sci. Technol.* 50 (7) (2016) 3866–3874.
- [28] X. Lu, Y. Peng, L. Ge, R. Lin, Z. Zhu, S. Liu, Amphiphobic PVDF composite membranes for anti-fouling direct contact membrane distillation, *J. Membr. Sci.* 505 (2016) 61–69.
- [29] Z. Wang, J. Jin, D. Hou, S. Lin, Tailoring surface charge and wetting property for robust oil-fouling mitigation in membrane distillation, *J. Membr. Sci.* 516 (2016) 113–122.
- [30] J. Zeng, Z. Guo, Superhydrophilic and underwater superoleophobic MFI zeolite-coated film for oil/water separation, *Colloids Surf. A: Physicochem. Eng. Asp.* 444 (2014) 283–288.
- [31] J. Yang, H. Song, X. Yan, H. Tang, C. Li, Superhydrophilic and superoleophobic chitosan-based nanocomposite coatings for oil/water separation, *Cellulose* 21 (3) (2014) 1851–1857.
- [32] J. Li, L. Yan, W. Li, J. Li, F. Zha, Z. Lei, Superhydrophilic-underwater superoleophobic ZnO-based coated mesh for highly efficient oil and water separation, *Mater. Lett.* 153 (2015) 62–65.
- [33] J. Ju, T. Wang, Q. Wang, Superhydrophilic and underwater superoleophobic PVDF membranes via plasma-induced surface PEGDA for effective separation of oil-in-water emulsions, *Colloids Surf. A: Physicochem. Eng. Asp.* 481 (2015) 151–157.
- [34] T. Yuan, J. Meng, T. Hao, Z. Wang, Y. Zhang, A scalable method toward superhydrophilic and underwater superoleophobic PVDF membranes for effective oil/water emulsion separation, *ACS Appl. Mater. Interfaces* 7 (27) (2015) 14896–14904.
- [35] C. Zhou, J. Cheng, K. Hou, A. Zhao, P. Pi, X. Wen, S. Xu, Superhydrophilic and

- underwater superoleophobic titania nanowires surface for oil repellency and oil/water separation, *Chem. Eng. J.* 301 (2016) 249–256.
- [36] L. Liu, C. Chen, S. Yang, H. Xie, M. Gong, X. Xu, Fabrication of superhydrophilic-underwater superoleophobic inorganic anti-corrosive membranes for high-efficiency oil/water separation, *Phys. Chem. Chem. Phys.* 18 (2) (2016) 1317–1325.
- [37] T. Chen, M. Duan, S. Fang, Fabrication of novel superhydrophilic and underwater superoleophobic hierarchically structured ceramic membrane and its separation performance of oily wastewater, *Ceram. Int.* 42 (7) (2016) 8604–8612.
- [38] G. Zuo, R. Wang, Novel membrane surface modification to enhance anti-oil fouling property for membrane distillation application, *J. Membr. Sci.* 447 (2013) 26–35.
- [39] C. Zhang, Y. Ou, W.-X. Lei, L.-S. Wan, J. Ji, Z.-K. Xu, CuSO<sub>4</sub>/H<sub>2</sub>O<sub>2</sub>-induced rapid deposition of polydopamine coatings with high uniformity and enhanced stability, *Angew. Chem. – Int. Ed.* 55 (9) (2016) 3054–3057.
- [40] Z.-X. Wang, C.-H. Lau, N.-Q. Zhang, Y.-P. Bai, L. Shao, Mussel-inspired tailoring of membrane wettability for harsh water treatment, *J. Mater. Chem. A* 3 (6) (2015) 2650–2657.
- [41] H.-C. Yang, K.-J. Liao, H. Huang, Q.-Y. Wu, L.-S. Wan, Z.-K. Xu, Mussel-inspired modification of a polymer membrane for ultra-high water permeability and oil-in-water emulsion separation, *J. Mater. Chem. A* 2 (26) (2014) 10225–10230.
- [42] H.-C. Yang, J.-K. Pi, K.-J. Liao, H. Huang, Q.-Y. Wu, X.-J. Huang, Z.-K. Xu, Silica-decorated polypropylene microfiltration membranes with a mussel-inspired intermediate layer for oil-in-water emulsion separation, *ACS Appl. Mater. Interfaces* 6 (15) (2014) 12566–12572.
- [43] H. Ma, P. Gao, Y. Zhang, D. Fan, G. Li, B. Du, Q. Wei, Engineering microstructured porous films for multiple applications via mussel-inspired surface coating, *RSC Adv.* 3 (47) (2013) 25291–25295.
- [44] Z. Wang, X. Jiang, X. Cheng, C.H. Lau, L. Shao, Mussel-inspired hybrid coatings that transform membrane hydrophobicity into high hydrophilicity and underwater superoleophobicity for oil-in-water emulsion separation, *ACS Appl. Mater. Interfaces* 7 (18) (2015) 9534–9545.
- [45] W.-Z. Qiu, H.-C. Yang, L.-S. Wan, Z.-K. Xu, Co-deposition of catechol/polyethyleneimine on porous membranes for efficient decolorization of dye water, *J. Mater. Chem. A* 3 (27) (2015) 14438–14444.
- [46] Y.-S. Choi, H. Kang, D.-G. Kim, S.-H. Cha, J.-C. Lee, Mussel-inspired dopamine- and plant-based cardanol-containing polymer coatings for multifunctional filtration membranes, *ACS Appl. Mater. Interfaces* 6 (23) (2014) 21297–21307.
- [47] C. Cheng, S. Li, W. Zhao, Q. Wei, S. Nie, S. Sun, C. Zhao, The hydrodynamic permeability and surface property of polyethersulfone ultrafiltration membranes with mussel-inspired polydopamine coatings, *J. Membr. Sci.* 417–418 (2012) 228–236.
- [48] Y. Lv, H.-C. Yang, H.-Q. Liang, L.-S. Wan, Z.-K. Xu, Nanofiltration membranes via co-deposition of polydopamine/polyethyleneimine followed by cross-linking, *J. Membr. Sci.* 476 (2015) 50–58.
- [49] G. Han, S. Zhang, X. Li, N. Widjojo, T.-S. Chung, Thin film composite forward osmosis membranes based on polydopamine modified polysulfone substrates with enhancements in both water flux and salt rejection, *Chem. Eng. Sci.* 80 (2012) 219–231.
- [50] F. Li, Q. Cheng, Q. Tian, B. Yang, Q. Chen, Biofouling behavior and performance of forward osmosis membranes with bioinspired surface modification in osmotic membrane bioreactor, *Bioresour. Technol.* 211 (2016) 751–758.
- [51] H.C. Yang, J. Hou, V. Chen, Z.K. Xu, Janus membranes: exploring duality for advanced separation, *Angew. Chem. – Int. Ed.* 55 (43) (2016) 13398–13407.
- [52] H. Li, L. Peng, Y. Luo, P. Yu, Enhancement in membrane performances of a commercial polyamide reverse osmosis membrane via surface coating of polydopamine followed by the grafting of polyethyleneimine, *RSC Adv.* 5 (119) (2015) 98566–98575.
- [53] H. Shi, L. Xue, A. Gao, Y. Fu, Q. Zhou, L. Zhu, Fouling-resistant and adhesion-resistant surface modification of dual layer PVDF hollow fiber membrane by dopamine and quaternary polyethyleneimine, *J. Membr. Sci.* 498 (2016) 39–47.
- [54] X. Yang, R. Wang, A.G. Fane, Novel designs for improving the performance of hollow fiber membrane distillation modules, *J. Membr. Sci.* 384 (1–2) (2011) 52–62.
- [55] H.M. Park, W.M. Lee, Helmholtz-Smoluchowski velocity for viscoelastic electro-osmotic flows, *J. Colloid Interface Sci.* 317 (2) (2008) 631–636.
- [56] Y. Wu, S. Iglauer, P. Shuler, Y. Tang, W.A. Goddard, Alkyl polyglycoside-sorbitan ester formulations for improved oil recovery, *Tenside Surfactants Deterg.* 47 (5) (2010) 280–287.
- [57] P.M. Kruglyakov, *Hydrophile – Lipophile Balance of Surfactants and Solid Particles: Physicochemical Aspects and Applications*, Elsevier Science, Amsterdam, Netherlands, 2000.
- [58] Z.E. Proverbio, S.M. Bardavid, E.L. Arancibia, P.C. Schulz, Hydrophile-lipophile balance and solubility parameter of cationic surfactants, *Colloids Surf. A: Physicochem. Eng. Asp.* 214 (1–3) (2003) 167–171.
- [59] R.N. Wenzel, Resistance of solid surfaces to wetting by water, *Ind. Eng. Chem.* 28 (8) (1936) 988–994.
- [60] L. Wang, F. Fang, Y. Liu, J. Li, X. Huang, Facile preparation of heparinized polysulfone membrane assisted by polydopamine/polyethyleneimine co-deposition for simultaneous LDL selectivity and biocompatibility, *Appl. Surf. Sci.* 385 (2016) 308–317.
- [61] E. Herlinger, R.F. Jameson, W. Linert, Spontaneous autoxidation of dopamine, *J. Chem. Soc. Perkin Trans. 2* (2) (1995) 259–263.
- [62] J. Liebscher, R. Mrowczynski, H.A. Scheidt, C. Filip, N.D. Haidade, R. Turcu, A. Bende, S. Beck, Structure of polydopamine: a never-ending story? *Langmuir* 29 (33) (2013) 10539–10548.
- [63] N.F. Della Vecchia, R. Avolio, M. Alfe, M.E. Errico, A. Napolitano, M. D’Ischia, Building-block diversity in polydopamine underpins a multifunctional eumelanin-type platform tunable through a quinone control point, *Adv. Funct. Mater.* 23 (10) (2013) 1331–1340.
- [64] A.N. Pham, T.D. Waite, Cu(II)-catalyzed oxidation of dopamine in aqueous solutions: mechanism and kinetics, *J. Inorg. Biochem.* 137 (2014) 74–84.
- [65] D.B. Knorr, N.T. Tran, K.J. Gaskell, J.A. Orlicki, J.C. Woicik, C. Jaye, D.A. Fischer, J.L. Lenhart, Synthesis and characterization of aminopropyltriethoxysilane-polydopamine coatings, *Langmuir* 32 (17) (2016) 4370–4381.
- [66] S. Saidin, P. Chevallier, M.R. Abdul Kadir, H. Hermawan, D. Mantovani, Polydopamine as an intermediate layer for silver and hydroxyapatite immobilisation on metallic biomaterials surface, *Mater. Sci. Eng.: C (Mater. Biol. Appl.)* 33 (8) (2013) 4715–4724.
- [67] H.-C. Yang, W. Xu, Y. Du, J. Wu, Z.-K. Xu, Composite free-standing films of polydopamine/polyethyleneimine grown at the air/water interface, *RSC Adv.* 4 (85) (2014) 45415–45418.
- [68] N.G.P. Chew, S. Zhao, C.H. Loh, N. Permogorov, R. Wang, Surfactant effects on water recovery from oil-in-water emulsions via direct-contact membrane distillation, *J. Membr. Sci.* 528 (2017) 126–134.
- [69] B. Kronberg, K. Holmberg, B. Lindman, *Surface Chemistry of Surfactants and Polymers*, John Wiley & Sons, United Kingdom, 2014.
- [70] P.-J. Lin, M.-C. Yang, Y.-L. Li, J.-H. Chen, Prevention of surfactant wetting with agarose hydrogel layer for direct contact membrane distillation used in dyeing wastewater treatment, *J. Membr. Sci.* 475 (2015) 511–520.
- [71] R. Meszaros, L. Thompson, M. Bos, I. Varga, T. Gilanyi, Interaction of sodium dodecyl sulfate with polyethyleneimine: surfactant-induced polymer solution colloid dispersion transition, *Langmuir* 19 (3) (2003) 609–615.
- [72] H. Wang, Y. Wang, H. Yan, J. Zhang, R.K. Thomas, Binding of sodium dodecyl sulfate with linear and branched polyethyleneimines in aqueous solution at different pH values, *Langmuir* 22 (4) (2006) 1526–1533.
- [73] S. Chen, L. Li, C. Zhao, J. Zheng, Surface hydration: principles and applications toward low-fouling/nonfouling biomaterials, *Polymer* 51 (23) (2010) 5283–5293.
- [74] S. Chen, F. Yu, Q. Yu, Y. He, S. Jiang, Strong resistance of a thin crystalline layer of balanced charged groups to protein adsorption, *Langmuir* 22 (19) (2006) 8186–8191.